Computational Study of Kinematics of the Anterior Cruciate Ligament Double-Bundle Structure during Passive Knee Flexion–Extension

Tomohiro Otani[a,*], Yo Kobayashi[a], Masao Tanaka[a]

[a] *Department of Mechanical Science and Bioengineering, Graduate School of Engineering Science, Osaka University, Toyonaka, Osaka, 560-8531, Japan*

Word count: 3303

*Corresponding author
Email address: `otani@me.es.osaka-u.ac.jp` (Tomohiro Otani)

Abstract

The anterior cruciate ligament (ACL) comprises an anteromedial bundle (AMB) and posterolateral bundle (PLB). Cadaver studies showed that this double-bundle structure exhibits reciprocal function during passive knee flexion–extension, with the PLB taut in knee extension and the AMB taut in knee flexion. *In vivo* measurements indicated that straight-line lengths of both bundles decrease with increasing knee-flexion angle (KFA). To interpret these seemingly conflicting facts, we developed a computational ACL model simulating the kinematics of the double-bundle structure during passive knee flexion–extension. Tibial and femoral shapes were reconstructed from computed-tomography images of a cadaver knee and used to construct an idealized model of an ACL including its bundles at the tibiofemoral joint. The ACL deformations at various KFAs were computed by finite element analysis. Results showed that the PLB was stretched in knee extension (KFA $= 0°$) and slackened with increasing KFA. The AMB was stretched in knee extension (KFA $= 0°$) and remained stretched on the medial side when the knee flexed (KFA $= 90°$), but its straight-line length decreased with increasing KFA. These findings are consistent with cadaver and *in vivo* experimental results and highlight the usefulness of a computational approach for understanding ACL functional anatomy.

keyword

Anterior Cruciate Ligament, Functional anatomy, Passive knee flexion–extension, Double-bundle structure, Finite element method.

1. Introduction

The anterior cruciate ligament (ACL) is one of four essential knee-joint ligaments that stabilize the joint, especially in the anterior drawer. ACL injury is one of the most common knee-joint injuries and often occurs without contact [1]. Many biomechanical studies of the ACL from various viewpoints (*e.g.,* functional anatomy, mechanical properties) have been conducted to better understand the mechanism of ACL injuries and to improve ACL reconstruction techniques, as shown in recent review articles [2, 3].

According to existing cadaver studies about ACL functional anatomy [4, 5, 6], the ACL structure can be divided into two fiber bundles located on the anteromedial side (anteromedial bundle; AMB) and the posterolateral side (posterolateral bundle; PLB). It is commonly believed that this fiber double-bundle structure has a reciprocal relation in that the PLB is tensed in knee extension, and the AMB is tensed in knee flexion. Recent *in vivo* three-dimensional imaging measurements revealed that the straight-line lengths of both bundles were longest at low knee flexion angles (KFAs) and shortened significantly with an increasing KFA. Based on their *in vivo* experimental results [7, 8, 9, 10], Jordan *et al.* [8] noted that the function of these two bundles may be better characterized as complementary, rather than reciprocal.

To interpret these seemingly conflicting facts and deepen our understanding of the function of the double-bundle structure, we hypothesized that a computational approach to expressing the ACL deformation and kinematics of the double-bundle structure in the mechanical sense might be a powerful approach. Various computational ACL models have been proposed [11, 12] following earlier computational three-dimensional (3D) ACL models with anisotropic properties exhibited by the fiber orientation to represent the stress field in the ACL during passive knee flexion–extension [13, 14]. In the past decade, greatly advanced simulations were used in studies that considered other ligaments and cartilage as well [15, 16]. However, knowledge about the function of the ACL double-bundle structure is still limited, and there is still great interest in improving the means to reconstruct the ACL after injury [17]. Computational simulation based on existing computational mechanical ACL models and recently gained anatomical knowledge may help us interpret experimental facts and update our understanding of the function of the ACL double-bundle structure.

This study therefore aimed to develop a computational ACL model to express the kinematics of the ACL double-bundle structure during passive knee flexion–extension. Tibial and femoral shapes were extracted from computed-tomography (CT) images, and their postures at various KFAs were represented based on recent *in vivo* measurements. A computational ACL model with its double-bundle structure was then set up as a tibiofemoral joint. Its deformation under prescribed postures at various KFAs was then calculated by a finite element method. The fiber orientation of the double-bundle structure and its deformations were then evaluated based on the computational results.

2. Materials and Methods

2.1. Tibiofemoral joint kinematics

To represent the tibiofemoral joint geometry and its postures during passive knee flexion–extension, the right femur and tibia geometries (supine position) were extracted from representative CT images of a female cadaver that are archived in the Visible Human Project [18] using ScanIP version 7.0 (Synopsys; Mountain View, CA, USA) (Figure 1 (a)). Insertion sites of the ACL at each bone—–Γ_t on the tibia and Γ_f on the femur—–were modeled as ovals [19], in which the sizes of the major axis [mm] and minor axis [mm] were set at 8.0:5.5 in Γ_t and 7.5:5.0 in Γ_f with consideration of the AMB and PLB positions [20, 21].

The femoral and tibial postures at various KFAs were expressed based on the functional flexion axis (FFA), in which the knee flexion–extension is expressed as rotations around two body-embedded axes (the flexion–extension and internal–external (IE) rotation axes) [22, 23]. The surgical trans-epicondylar axis in the femur was set based on *in vivo* measurements of knee-joint kinematics conducted by Asano *et al.* [24] and used as the flexion–extension axis (Fig. 1(b) top). The longitudinal rotation axis was set based on previous cadaver studies [23, 25] and used as the IE rotation axis (Fig. 1(b) bottom) at low KFAs (screw-home movement). The IE rotation was considered at low KFAs ($<= 30°$) [23] and expressed as the internal rotation of the tibia by a constant fraction with increasing KFA. The range of the IE rotation θ_{IE} [°] was 30° based on previous experimental measurements [26, 23]. Additionally, the anterior–posterior (AP) displacement of the femur was used to describe its sliding motion on the tibial plateau at high KFAs (*e.g.,* as shown in [24, 27]). The AP displacement was considered at high KFAs ($> 45°$) and expressed as femoral displacement to the posterior side of the tibial plateau proportionally with increasing KFA. The total AP displacement, l_{AP} [mm], was set to 10 mm based on previous experimental observations [24].

To evaluate the effects of the degrees of IE rotation and AP displacement on the femoral and tibial postures associated with the ACL kinematics, parametric studies of the AP displacement and IE rotation were conducted, and the results were compared with the straight-line lengths of the AMB and PLB. First, the degrees of IE rotation in three cases, $\theta_{\mathrm{IE}} = 30°$, $15°$, and $0°$, with a constant l_{AP} of 10 mm were compared. Next, the degrees of AP displacement in three cases, $l_{\mathrm{AP}} = 10$, 5, and 0 mm with a constant θ_{IE} of $30°$ were compared.

2.2. ACL geometry construction

An ACL model with the double-bundle structure was constructed (Fig.1(d)). The initial geometry of the ACL was constructed to interpolate insertion sites on the tibia, Γ_t, and femur, Γ_f, at a KFA of $90°$, when the straight-line length of the ACL was shortest. ACL reference geometry was constructed by in-plane rotation of both insertion sites of the initial ACL geometry to parallel the double-bundle structure. The ACL reference geometry was discretized by a set of eight-node hexahedral elements, consisting of 18,880 elements with

20,459 nodes.

Fiber orientations of each bundle were defined by the method of Otani and Tanaka [28] to assign unit direction vectors of fibers. In each bundle, the fiber direction vector, **a**, was defined as the unit vector of the spatial gradient of the scalar variable, ϕ, which is given by

$$\mathbf{a} = \frac{\nabla\phi}{\|\nabla\phi\|}. \tag{1}$$

The spatial distribution of ϕ was modeled to be smooth and was expressed by solving the Laplace equation in each bundle while following the Dirichlet boundary condition ($\phi = 1$ on Γ_t and $\phi = 0$ on Γ_f).

2.3. Computation of ACL deformation

We simulated ACL deformation at various KFAs using the ACL model of Weiss *et al.* [29], which can express nearly incompressible, transversely isotropic properties of the ACL. The strain energy density function W was described by the following three terms:

$$W = W_{\text{iso}}(\hat{I}_1) + W_{\text{aniso}}(\lambda) + W_{\text{vol}}(J) \tag{2}$$

where W_{iso} and W_{aniso} are the chronic components that express the isotropic and anisotropic characteristics, respectively. W_{iso} and W_{aniso} are given by

$$W_{\text{iso}}(\hat{I}_1) = c_1(\hat{I}_1 - 3) \tag{3}$$

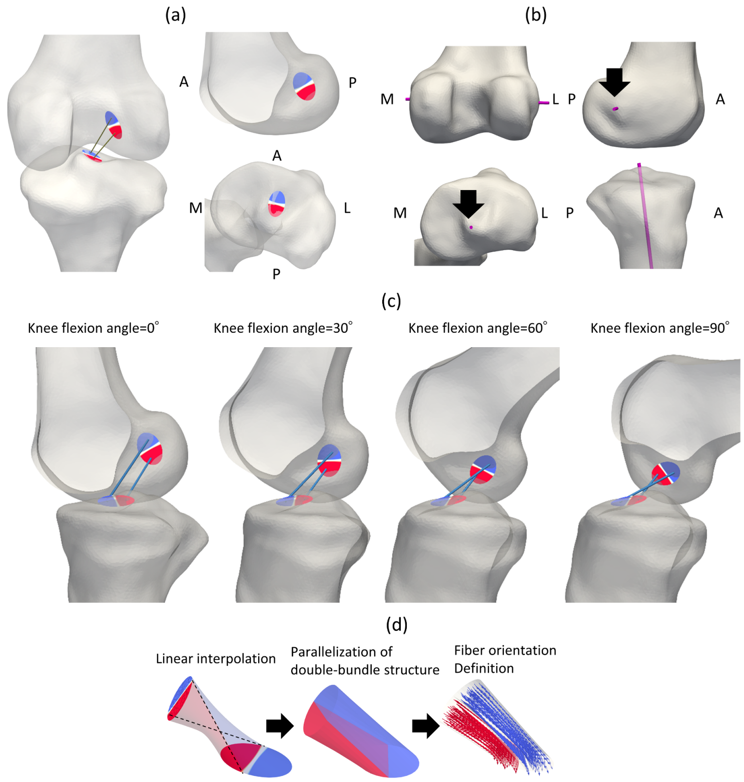

Figure 1: Workflow representing the geometries and postures of a tibiofemoral joint with the anterior cruciate ligament (ACL). (a) Femoral and tibial shapes extracted from computed-tomography images with the ACL insertion sites, including the anteromedial bundle (AMB, blue) and posterolateral bundle (PLB, red). (b) Axes of knee flexion–extension for the femur and interior–exterior rotation of the tibia. (c) Postures of the tibiofemoral joint at knee flexion angles of 0°, 30°, 60°, and 90° (viewed from the medial side). (d) Reference geometry construction of the ACL and definition of fiber orientation in the double bundle. Initially, the ACL geometry was represented by linear interpolation between insertion sites at a knee-flexion angle of 90°, when the straight-line length of the ACL was shortest (left). The ACL reference geometry was constructed by in-plane rotation of both insertion sites in the initial ACL geometry to parallel the double-bundle structure (center). The fiber orientations of each bundle were defined by the method presented by Otani and Tanaka [28] (right).

$$\lambda \frac{\partial W_{\text{aniso}}}{\partial \lambda} = \begin{cases} 0 & \text{if } \lambda < 1 \\ c_3[\exp[c_4(\lambda - 1)]] & \text{if } 1 \leq \lambda \leq \lambda^* \\ c_5\lambda + c_6 & \text{Otherwise} \end{cases} \tag{4}$$

where c_1, c_3, c_4, c_5, and c_6 are constants, and λ^* is the threshold used to determine the phenomenological properties of the bundles. These terms were established by the modified first invariants of the right Cauchy–-Green deformation tensor, $\hat{I}_1 = \text{tr}(\hat{\mathbf{C}})$, and the stretch ratio expressing the deformation along the orientations of the fiber bundles, $\lambda = \sqrt{\mathbf{a}^T \cdot \mathbf{C} \cdot \mathbf{a}}$. Here, $\hat{\mathbf{C}}$ represents the modified right Cauchy–Green deformation tensor and is expressed as $J^{-\frac{2}{3}}\mathbf{C}$ based on the volume ratio, J, and the right Cauchy–Green deformation tensor, $\mathbf{C}$. The volumetric component, W_{vol}, is expressed in terms of J as follows:

$$W_{\text{vol}}(J) = k_v \ln J^2 \tag{5}$$

where k_v is the penalty parameter. The values of these parameters were set as described by Pena *et al.* [30] and calculated by fitting the experimental measurements reported by Butler *et al.* [31].

The ACL deformations at various KFAs were calculated by solving the weak form of the equilibrium equation using the Galerkin finite element method with the Newton–Raphson scheme (*cf.* [32]). Selective reduced integration was applied to alleviate volume locking. The linearized equation was calculated by PARDISO implemented in the Intel Math Kernel Library.

The initial stretch ratio was set for each bundle using the method of Limbert *et al.* [14] to avoid non-physiological fiber extension. In this study, the initial stretch ratio was assumed to be uniform for each bundle and was set at 0.75 for the AMB and at 0.7 for the PLB, not to exceed the failure limit of the ACL— that is, 1.2, based on Butler *et al.* [33]—regardless of the KFA.

3. Results

3.1. ACL kinematics during passive knee flexion-extension

Figure 2(a) and (b) show the motion of the femur relative to the tibia and the surgical trans-epicondylar axis for KFAs from 0° to 90°. The tibiofemoral joint motion indicates that the posterior displacement of the lateral condyle was higher than that of the medial condyle, which is well-known behavior based on *in vivo* and *in vitro* measurements (*e.g.,* [34, 35]). The changes in the ACL bundle lengths in the above case for KFAs from 0° to 90° are shown as black lines in Fig. 2(c). Both the AMB and PLB lengths were within the ranges observed thorugh *in vivo* measurements by Yoo *et al.* [9] at KFAs of 45° and 90°.

Furthermore, the effects of the degrees of AP displacement and IE rotation were evaluated by parametric studies about l_{AP} and θ_{IE}. As l_{AP} decreased to 5 and 0 mm, the AMB was shortened, and the AP displacement decreased; these lengths were outside the range of the *in vivo* measurements reported by Yoo *et al.* [9] at a KFA of 90°. However, the decreases in the

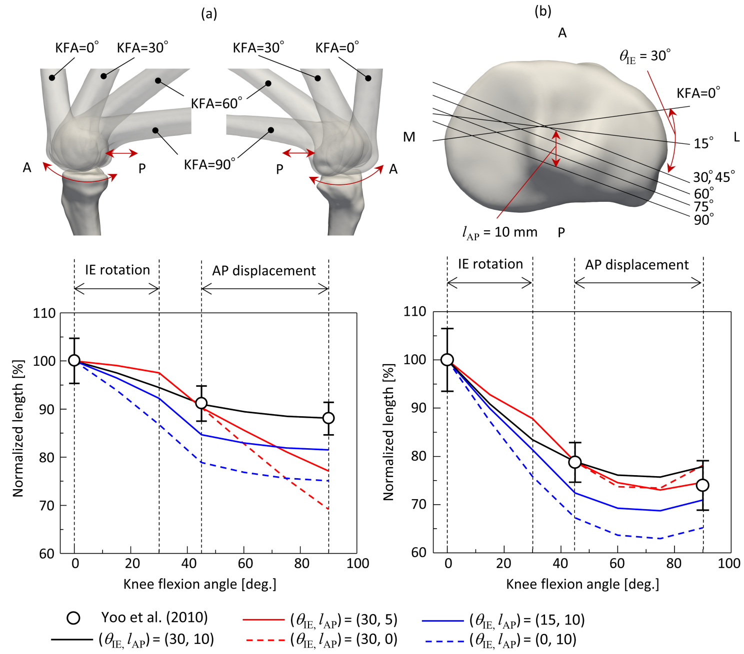

Figure 2: Tibial and femoral postures during knee flexion angle (KFA) from 0° to 90°. Representative postures of the tibiofemoral joint at KFAs of 0°, 30°, 60°, and 90° (a) and movement of the surgical epicondylar axis for KFA from 0° to 90° (b) for a total IE rotation angle of 30° and AP displacement of 10 mm. (c) Normalized lengths of the anteromedial bundle (AMB, left) and posterolateral bundle (PLB, right) at KFAs from 0° to 90° with various degrees of the internal–external rotation, θ_{IE}, and AP displacement, l_{AP}. *In vivo* experimental data (open circles) [9] are shown for comparison.

PLB length were consistent regardless of the AP displacement and remained within the range of the *in vivo* measurements reported by Yoo *et al.* [9] in all cases. When θ_{IE} was decreased to 15° and 0°, although both the AMB and PLB lengths reduced similarly in all cases, the reduction ratios increased with decreasing θ_{IE}. These values were out of the range of the *in vivo* measurements reported by Yoo *et al.* [9] except for the case in which $\theta_{\mathrm{IE}} = 15°$ and KFA $= 90°$.

3.2. ACL fiber orientations

Snapshots of the ACL geometry, fiber orientation of each bundle, and stretch ratios at KFAs of 0°, 30°, 60°, and 90° are shown in Fig. 3. The fiber orientation was visually represented as tangential lines showing the direction vectors of fibers. The double-bundle structures in the ACL were almost parallel at a KFA of 0° and became twisted and curved when the knee flexed. The stretch ratio of the PLB in the posteromedial side was locally $\lambda >$ 100% at a KFA of 0° and decreased with increasing KFA. Almost all domains in the PLB slackened ($\lambda < 100\%$) even at a KFA of 30°. The stretch ratios of the AMB on the medial side were also $\lambda > 100\%$ regardless of the KFA, whereas those on the lateral side were relatively low and slackened when the knee flexed.

To evaluate the extents of the two bundle stretches quantitatively, we calculated the volume fraction of the stretch ratio in each bundle domain (Fig. 4). Approximately 50% of each bundle had stretched ($\lambda > 100\%$) when the KFA was 0°. In the PLB, the slackened domain ($\lambda < 100\%$) consistently increased with increasing KFA, and almost all domains had slackened at a KFA of 90°. In the AMB, the degree of stretching became relatively mild at a KFA of 30°, and approximately 38% of the AMB domain was stretched ($\lambda > 100\%$); the domain remained stretched regardless of the KFA. The AMB had the least stretched domain (approximately 23%) at a KFA of 60°, and it was approximately 29% at a KFA of 90°.

Finally, we considered the influences of the AP displacement and IE ro-

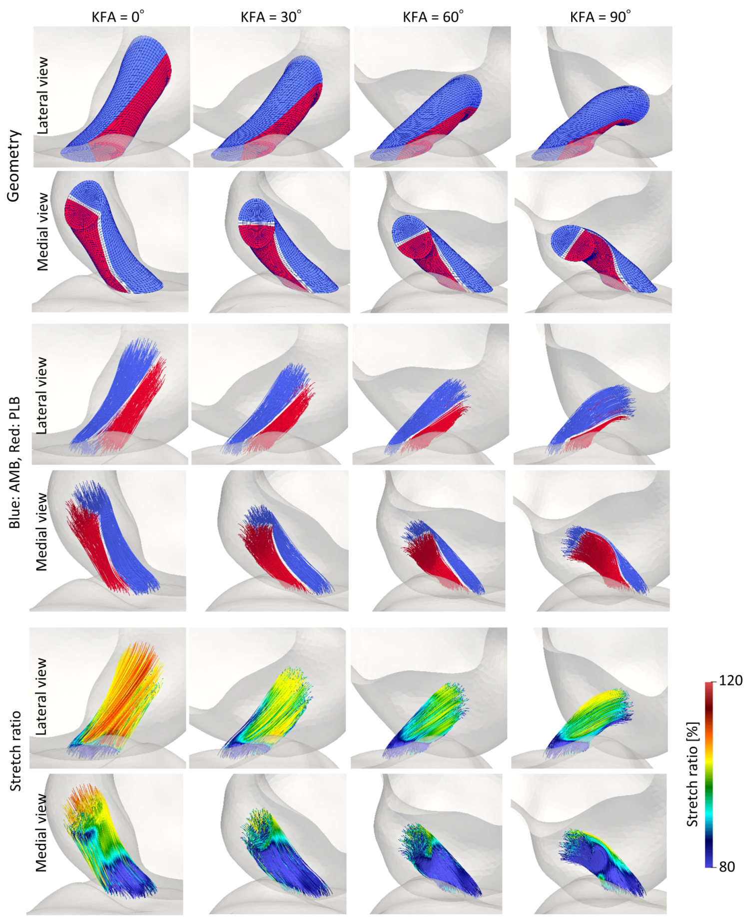

Figure 3: Geometry of the anterior cruciate ligament (ACL, top), fiber orientations of the anteromedial bundle (AMB) and posterolateral bundle (PLB) (middle), and fiber stretch ratios, λ (bottom), at knee flexion angles of 0°, 30°, 60°, and 90° (viewed from the medial and lateral sides). The fiber orientation is represented as tangential lines along the fiber direction vectors, and the fiber stretch ratios are visualized on these tangential lines.

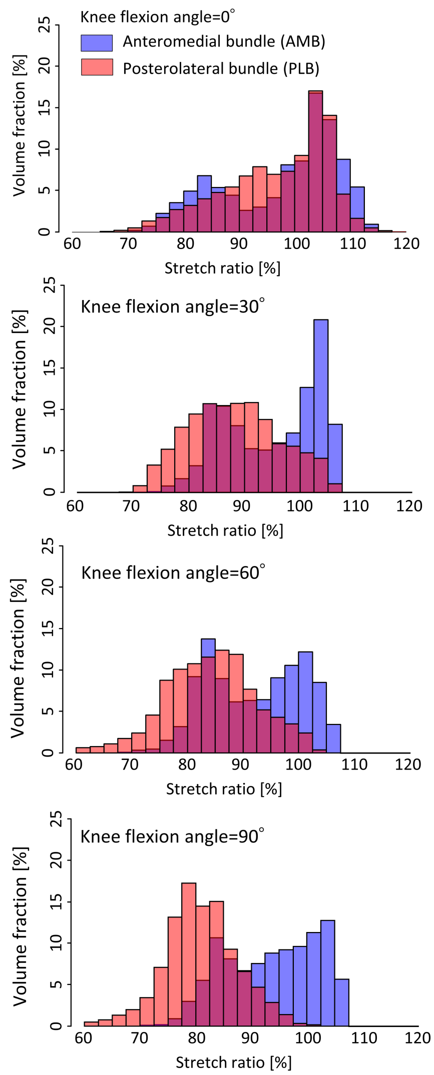

Figure 4: Volume fractions of the stretch ratios in the anteromedial bundle (AMB, blue) and posterolateral bundle (PLB, red) at knee flexion angles of 0° (top), 30° (top middle), 60° (bottom middle), and 90° (bottom).

tation on the ACL deformation. The ACL deformations in the flexion states relative to the fully extended state (KFA = 0°) were computed for two cases: small $l_{\mathrm{AP}} = 5$ mm with $\theta_{\mathrm{IE}} = 30°$ and small $\theta_{\mathrm{IE}} = 15°$ with $l_{\mathrm{AP}} = 10$ mm. Figure 5 (a) shows the volume fraction of the stretch ratio in each bundle domain at a KFA of 90° in each case. Although the PLB domain was almost slack (stretch ratio < 100%) in the case of $(\theta_{\mathrm{IE}}, l_{\mathrm{AP}}) = (30, 10)$ (Fig. 4 (bottom)), the PLB domain was still partially stretched (stretch ratio > 100%) in in the cases of $(\theta_{\mathrm{IE}}, l_{\mathrm{AP}}) = (30, 5)$ and (15, 10).

To evaluate the differences between the ACL deformation states in the above computations, we evaluated the changes in the AMB and PLB ridge lengths, which were defined as connections between the major vertexes of the insertion sites along the ACL (black lines in Fig. 5 (b)). Figure 5 (c) shows the changes in the AMB and PLB ridge lengths from KFAs from 0° to 90° in each case. The length of the AMB ridge line was almost constant during knee flexion in all cases. However, the length of the PLB ridge line monotonically decreased with increasing KFA and fell below 80% when KFA = 90° in the case of $(\theta_{\mathrm{IE}}, l_{\mathrm{AP}}) = (30, 10)$, but increased with increasing KFA from 45°, approaching 90% when KFA = 90° in other cases.

4. Discussion

The function of the ACL double-bundle structure has been of great interest, with various experimental studies having evaluated its functional anatomy [36]. Results of earlier cadaveric studies have been interpreted as

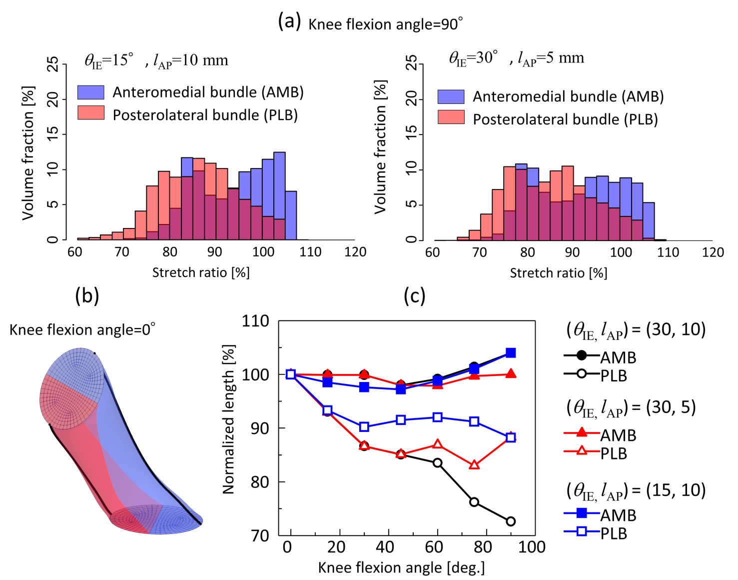

Figure 5: (a) Volume fraction of the stretch ratio in the anteromedial bundle (AMB, blue) and the posterolateral bundle (PLB, red) at knee flexion angles of 90° in the case that $(\theta_{\mathrm{IE}}, l_{\mathrm{AP}})$= (30, 5) (left) and (15, 10) (right). (b) The AMB and PLB domains are shown in blue and red, respectively. (c) Normalized lengths of the AMB and PLB ridges (black lines in (b)) as the KFA increased from 0° to 75°.

showing that the double-bundle structure functions reciprocally, such that the PLB is taut in knee extension, and AMB is taut in knee flexion [4, 5, 6]. Recent *in vivo* measurements showed that both bundles are longest at full knee extension [7, 8, 9, 10]. Amis [36] summarized these facts and noted that AMB is close to isometric when the knee flexes, whereas the PLB slackens.

The present study developed a computational ACL model to represent the kinematics of the ACL double-bundle structure during passive knee flexion–extension based on recent *in vivo* measurements. The results showed that the PLB was stretched at full knee extension and slackened when the knee flexed. In contrast, the AMB was continuously taut, especially on the medial side, regardless of the KFA, although the straight-line length of the AMB monotonically decreased with increasing KFA. This apparently isometric behavior of the AMB can be explained by a torsional deformation of the ACL determined by the relative positional relation between the insertion sites on the tibiofemoral joint (Fig. 3). This result is consistent with those of both cadaver and *in vivo* experimental results. This finding also shows that the function of the double-bundle structure of the ACL is associated with the 3D kinematics of the insertion sites on the femur and tibia.

Furthermore, the effects of the IE rotation and AP displacement on the kinematics of the ACL bundles during knee flexion were evaluated. Results showed that small degrees of IE rotation and AP displacement made the reduction in the bundle ridge lengths small (Fig 5) compared with the reduction in the straight-line lengths (Fig. 2) during knee flexion, which highlights its torsional deformation. This finding suggests that small degrees of IE rotation and AP displacement enhance the ACL torsional deformation, which may reduce the slack in the PLB when the knee is flexed (Fig. 5). The PLB slackness at high KFAs is well acknowledged from clinical measurements [36]. Thus, under normal conditions, these complex motions may act to reduce the load on the PLB when the knee is flexed against the torsional deformation of the ACL. However, the PLB might not be slackened, even at high KFAs, when the IE rotation and AP displacement are small. Therefore, the 3D ACL kinematics and deformation during knee flexion–extension should be considered in terms of the ACL length as well as its torsional deformation.

4.1. Limitations

In this study, we modeled the ACL kinematics using several simplifying assumptions based on previous studies. Therefore, the obtained results may have inconsistencies in terms of the subject-specific ACL kinematics. From this viewpoint, this study has two primary limitations. First, the subject-specific posture of the tibiofemoral joint at various KFAs was not considered in this study. Instead, we represented the femoral and tibial postures based on the FFA with consideration to the IE rotation and AP displacement. We conducted parametric studies of the effects of IE rotation and AP displacement on the tibiofemoral posture and confirmed anatomical consistency of represented postures in terms of the ACL kinematics. However, knee-joint motions vary widely due to subject-specific differences, measurement approaches, and FFA selection (*e.g.,* [37, 38]). Thus, it is still challenging to uniquely determine the knee-joint motion from tibiofemoral bone geometries. To overcome this issue and evaluate actual ACL kinematics during knee flexion–-extension, *in vivo* measurements of the kinematic relationship between the two ACL insertion sites would be useful. Second, we simplified the mechanical properties of the ACL, such as the reference geometry and fiber orientation of each bundle, due to incomplete anatomical knowledge. However, recent experimental studies showed that the microstructural properties and mechanics of each bundle are different [39, 40, 41, 42]. Thus, lack of knowledge about these mechanical properties makes computational evaluations of the mechanical stress field of the ACL challenging. To address this issue, further development of the ACL model that reflects the mechanical characteristics is strongly required.

The anatomical characteristics of the ACL double-bundle structure are still under debate in the medical field, and the ACL torsional deformation is central in the discussion of this issue. Śmigielski *et al.* [43] conducted a cadaveric study including 111 knees and concluded that the ACL forms a flat ribbon without a clear separation between the AMB and PLB . Following this finding, Noailles *et al.* [44] studied the geometric characteristics of the ACL using 60 cadaver knees and concluded that the torsion in the ACL fibers because of the relative position of bone insertions makes the ACL appear to have a double-bundle structure. Furthermore, Skelley *et al.* [41] reported that most of the microstructural and material properties of the ACL appear to follow a linear gradient across the ligament, rather than varying between bundles. Regarding this issue, our results show that torsional deformation can also occur when the AMB and PLB have different deformation characteristics. To bear this specific deformation, it may be reasonable that the AMB and PLB have different material properties. In future research, we plan to investigate the effects of spatial differences in the material properties of the ACL on its mechanical state during knee flexion—extension, which may contribute to the interpretation of recent ACL anatomical findings from a mechanical viewpoint.

5. Conclusions

This study computationally modeled ACL kinematics, focusing on its double-bundle structure, during passive knee flexion–extension. The results showed that the PLB was taut in knee extension, whereas the AMB was consistently taut, regardless of the KFA, although the straight-line length of AMB consistently decreased with increasing KFA. This apparently isometric behavior of the AMB can be explained by torsional deformation of the ACL determined by the relative positional relation between the insertion sites on the tibiofemoral joint. These results are consistent with existing experimental facts, and thus highlight the capabilities of the computational modeling to deepen our understanding of ACL kinematics and the functional anatomy of its double-bundle structure.

Acknowledgements

The authors thank Azumi Taoka for her efforts. The authors are grateful to the reviewers for their constructive comments, which were very helpful to improve the paper. The authors also thank Nancy Schatken, BS, MT (ASCP), from Edanz Group (www.edanzediting.com/ac), for editing a draft of this manuscript.

Conflict of interest

The authors have no financial or personal interests in the work reported in this paper.

Funding

None.

Ethical Approval

None.

References

[1] G. Myklebust, S. Maehlum, L. Engebretsen, T. Strand, E. Solheim, Registration of cruciate ligament injuries in Norwegian top level team handball. A prospective study covering two seasons, Scandinavian Journal of Medicine & Science in Sports 7 (5) (1997) 289–292. doi:10.1111/j.1600-0838.1997.tb00155.x.

[2] S. G. McLean, K. F. Mallett, E. M. Arruda, Deconstructing the Anterior Cruciate Ligament: What We Know and Do Not Know About Function, Material Properties, and Injury Mechanics, Journal of Biomechanical Engineering 137 (2) (2015) 020906. doi:10.1115/1.4029278.

[3] M. J. Anderson, W. M. Browning, C. E. Urband, M. A. Kluczynski, L. J. Bisson, A Systematic Summary of Systematic Reviews on the Topic of the Anterior Cruciate Ligament, Orthopaedic Journal of Sports Medicine 4 (3) (2016) 1–23. doi:10.1177/2325967116634074.

[4] A. A. Amis, G. P. Dawkins, Functional anatomy of the anterior cruciate ligament. Fibre bundle actions related to ligament replacements and injuries., The Journal of bone and joint surgery. British volume 73 (2) (1991) 260–7.

[5] F. Girgis, J. Marshall, A. Monajem, The Cruciate Ligaments of the Knee Joint: Anatomical. Functional and Experimental Analysis, Clinical Orthopaedics and Related Research (106) (1975) 216–31.

[6] T. Zantop, W. Petersen, J. K. Sekiya, V. Musahl, F. H. Fu, Anterior cruciate ligament anatomy and function relating to anatomical reconstruction, Knee Surgery, Sports Traumatology, Arthroscopy 14 (10) (2006) 982–992. doi:10.1007/s00167-006-0076-z.

[7] G. Li, L. E. DeFrate, H. Sun, T. J. Gill, In vivo elongation of the anterior cruciate ligament and posterior cruciate ligament during knee

flexion, American Journal of Sports Medicine 32 (6) (2004) 1415–1420. doi:10.1177/0363546503262175.

[8] S. S. Jordan, L. E. DeFrate, W. N. Kyung, R. Papannagari, T. J. Gill, G. Li, The in vivo kinematics of the anteromedial and posterolateral bundles of the anterior cruciate ligament during weightbearing knee flexion, American Journal of Sports Medicine 35 (4) (2007) 547–554. doi:10.1177/0363546506295941.

[9] Y. S. Yoo, W. S. Jeong, N. S. Shetty, S. J. M. Ingham, P. Smolinski, F. Fu, Changes in ACL length at different knee flexion angles: An in vivo biomechanical study, Knee Surgery, Sports Traumatology, Arthroscopy 18 (3) (2010) 292–297. doi:10.1007/s00167-009-0932-8.

[10] J. H. Wang, Y. Kato, S. J. M. Ingham, A. Maeyama, M. Linde-Rosen, P. Smolinski, F. H. Fu, Measurement of the end-to-end distances between the femoral and tibial insertion sites of the anterior cruciate ligament during knee flexion and with rotational torque, Arthroscopy 28 (10) (2012) 1524–1532. doi:10.1016/j.arthro.2012.03.004.

[11] F. Galbusera, M. Freutel, L. Dürselen, M. D'Aiuto, D. Croce, T. Villa, V. Sansone, B. Innocenti, Material Models and Properties in the Finite Element Analysis of Knee Ligaments: A Literature Review, Frontiers in Bioengineering and Biotechnology 2 (November) (2014) 1–11. doi:10.3389/fbioe.2014.00054.

[12] A. E. Peters, R. Akhtar, E. J. Comerford, K. T. Bates, Tissue material properties and computational modelling of the human tibiofemoral joint: a critical review, PeerJ 6 (2018) e4298. doi:10.7717/peerj.4298.

[13] S. Hirokawa, R. Tsuruno, Three-dimensional deformation and stress distribution in an analytical/computational model of the anterior cruciate ligament., Journal of biomechanics 33 (9) (2000) 1069–77.

[14] G. Limbert, M. Taylor, J. Middleton, Three-dimensional finite element modelling of the human ACL: Simulation of passive knee flexion with a stressed and stress-free ACL, Journal of Biomechanics 37 (11) (2004) 1723–1731. doi:10.1016/j.jbiomech.2004.01.030.

[15] A. D. Orsi, S. Chakravarthy, P. K. Canavan, E. Peña, R. Goebel, A. Vaziri, H. Nayeb-Hashemi, The effects of knee joint kinematics on anterior cruciate ligament injury and articular cartilage damage, Computer Methods in Biomechanics and Biomedical Engineering 19 (5) (2016) 493–506. doi:10.1080/10255842.2015.1043626.

[16] B. C. Marchi, E. M. Arruda, A study on the role of articular cartilage soft tissue constitutive form in models of whole knee biomechanics, Biomechanics and Modeling in Mechanobiology 16 (1) (2017) 117–138. doi:10.1007/s10237-016-0805-2.

[17] E. Hohmann, Editorial Commentary: The Ribbon Theory. Another Quantum Leap? The Anterior Cruciate Ligament Is Twisted and in

Fact a Flat Structure. Or not?, Arthroscopy - Journal of Arthroscopic and Related Surgery 33 (9) (2017) 1710–1711. doi:10.1016/j.arthro.2017.04.011.

[18] https://mri.radiology.uiowa.edu/visible_human_datasets.html.

[19] M. Odensten, J. Gillquist, Functional anatomy of the anterior cruciate ligament and a rationale for reconstruction., The Journal of bone and joint surgery. American volume 67 (2) (1985) 257–262.

[20] H. Otsubo, K. Shino, D. Suzuki, T. Kamiya, T. Suzuki, K. Watanabe, M. Fujimiya, T. Iwahashi, T. Yamashita, The arrangement and the attachment areas of three ACL bundles, Knee Surgery, Sports Traumatology, Arthroscopy 20 (1) (2012) 127–134. doi:10.1007/s00167-011-1576-z.

[21] E. K. Bicer, S. Lustig, E. Servien, T. A. S. Selmi, P. Neyret, Current knowledge in the anatomy of the human anterior cruciate ligament, Knee Surgery, Sports Traumatology, Arthroscopy 18 (8) (2010) 1075–1084. doi:10.1007/s00167-009-0993-8.

[22] A. M. Hollister, S. Jatana, A. K. Singh, W. W. Sullivan, A. G. Lupichuk, The axes of rotation of the knee, Clinical Orthopaedics and Related Research (290) (1993) 259–268. doi:10.1097/00003086-199305000-00033.

[23] D. L. Churchill, S. J. Incavo, C. C. Johnson, B. D. Beynnon, The transepicondylar axis approximates the optimal flexion axis of the knee, Clinical Orthopaedics and Related Research (356) (1998) 111–118. doi:10.1097/00003086-199811000-00016.

[24] T. Asano, M. Akagi, T. Nakamura, The functional flexion-extension axis of the knee corresponds to the surgical epicondylar axis: In vivo analysis using a biplanar image-matching technique, Journal of Arthroplasty 20 (8) (2005) 1060–1067. doi:10.1016/j.arth.2004.08.005.

[25] D. V. Boguszewski, N. B. Joshi, P. R. Yang, K. L. Markolf, F. A. Petrigliano, D. R. McAllister, Location of the natural knee axis for internal–external tibial rotation, Knee 23 (6) (2016) 1083–1088. doi:10.1016/j.knee.2015.11.003.

[26] L. Blankevoort, R. Huiskes, A. de Lange, The envelope of passive knee joint motion, Journal of Biomechanics 21 (9) (1988). doi:10.1016/0021-9290(88)90280-1.

[27] J. Victor, L. Labey, P. Wong, B. Innocenti, J. Bellemans, The influence of muscle load on tibiofemoral knee kinematics, Journal of Orthopaedic Research 28 (4) (2010) 419–428. doi:10.1002/jor.21019.

[28] T. Otani, M. Tanaka, Unloaded shape identification of human cornea by variational shape optimization, Computer Methods in Biomechanics

and Biomedical Engineering 21 (15) (2018) 795–802. doi:10.1080/10255842.2018.1521962.

[29] J. A. Weiss, B. N. Maker, S. Govindjee, Finite element implementation of incompressible, transversely isotropic hyperelasticity, Computer Methods in Applied Mechanics and Engineering 135 (1-2) (1996) 107–128. doi:10.1016/0045-7825(96)01035-3.

[30] E. Peña, B. Calvo, M. A. Martínez, M. Doblaré, A three-dimensional finite element analysis of the combined behavior of ligaments and menisci in the healthy human knee joint, Journal of Biomechanics 39 (9) (2006) 1686–1701. doi:10.1016/j.jbiomech.2005.04.030.

[31] D. L. Butler, M. Y. Sheh, D. C. Stouffer, V. A. Samaranayake, M. S. Levy, Surface strain variation in human patellar tendon and knee cruciate ligaments., Journal of biomechanical engineering 112 (1) (1990) 38–45.

[32] J. Bonet, R. D. Wood, Nonlinear continuum mechanics for finite element analysis, Cambridge University Press, 2008.

[33] D. L. Butler, Y. Guan, M. D. Kay, J. F. Cummings, S. M. Feder, M. S. Levy, Location-dependent variations in the material properties of the anterior cruciate ligament, Journal of Biomechanics 25 (5) (1992) 511–518. doi:10.1016/0021-9290(92)90091-E.

[34] H. Iwaki, V. Pinskerova, M. A. Freeman, Tibiofemoral movement 1: The shape and relative movements of the femur and tibia in the unloaded cadaver knee, Journal of Bone and Joint Surgery - Series B 82 (8) (2000) 1189–1195. doi:10.1302/0301-620X.82B8.10717.

[35] M. A. Freeman, V. Pinskerova, The movement of the normal tibio-femoral joint, Journal of Biomechanics 38 (2) (2005) 197–208. doi:10.1016/j.jbiomech.2004.02.006.

[36] A. A. Amis, The functions of the fibre bundles of the anterior cruciate ligament in anterior drawer, rotational laxity and the pivot shift, Knee Surgery, Sports Traumatology, Arthroscopy 20 (4) (2012) 613–620. doi:10.1007/s00167-011-1864-7.

[37] D. Eckhoff, C. Hogan, L. DiMatteo, M. Robinson, J. Bach, An ABJS best paper: Difference between the epicondylar and cylindrical axis of the knee, Clinical Orthopaedics and Related Research (461) (2007) 238–244. doi:10.1097/BLO.0b013e318112416b.

[38] T. Mochizuki, T. Sato, J. D. Blaha, O. Tanifuji, K. Kobayashi, H. Yamagiwa, S. Watanabe, Y. Koga, G. Omori, N. Endo, The clinical epicondylar axis is not the functional flexion axis of the human knee, Journal of Orthopaedic Science 19 (3) (2014) 451–456. doi:10.1007/s00776-014-0536-0.

[39] R. M. Castile, N. W. Skelley, B. Babaei, R. H. Brophy, S. P. Lake,

Microstructural properties and mechanics vary between bundles of the human anterior cruciate ligament during stress-relaxation, Journal of Biomechanics 49 (1) (2016) 87–93. doi:10.1016/j.jbiomech.2015.11.016.

[40] N. W. Skelley, R. M. Castile, T. E. York, V. Gruev, S. P. Lake, R. H. Brophy, Differences in the microstructural properties of the anteromedial and posterolateral bundles of the anterior cruciate ligament, American Journal of Sports Medicine 43 (4) (2015) 928–936. doi:10.1177/0363546514566192.

[41] N. W. Skelley, R. M. Castile, P. C. Cannon, C. I. Weber, R. H. Brophy, S. P. Lake, Regional Variation in the Mechanical and Microstructural Properties of the Human Anterior Cruciate Ligament, American Journal of Sports Medicine 44 (11) (2016) 2892–2899. doi:10.1177/0363546516654480.

[42] N. W. Skelley, S. P. Lake, R. H. Brophy, Microstructural properties of the anterior cruciate ligament, Annals of Joint 2 (2017) 19–19. doi:10.21037/aoj.2017.05.08.

[43] R. Śmigielski, U. Zdanowicz, M. Drwiega, B. Ciszek, B. Ciszkowska-Łysoń, R. Siebold, Ribbon like appearance of the midsubstance fibres of the anterior cruciate ligament close to its femoral insertion site: a cadaveric study including 111 knees, Knee Surgery, Sports

Traumatology, Arthroscopy 23 (11) (2015) 3143–3150. doi:10.1007/s00167-014-3146-7.

[44] T. Noailles, P. Boisrenoult, M. Sanchez, P. Beaufils, N. Pujol, Torsional Appearance of the Anterior Cruciate Ligament Explaining “Ribbon” and Double-Bundle Concepts: A Cadaver-based Study, Arthroscopy - Journal of Arthroscopic and Related Surgery 33 (9) (2017) 1703–1709. doi:10.1016/j.arthro.2017.03.019.